ADVANCED MATERIALS
www.advmat.de

# Surface Ligand Management Aided by a Secondary Amine Enables Increased Synthesis Yield of $CsPbI_3$ Perovskite Quantum Dots and High Photovoltaic Performance

*Yao Wang, Jianyu Yuan,* Xuliang Zhang, Xufeng Ling, Bryon W. Larson, Qian Zhao, Yingguo Yang, Yao Shi, Joseph M. Luther, and Wanli Ma**

**Lead-halide perovskite quantum dots (PQDs) or more broadly, nanocrystals possess advantageous features for solution-processed photovoltaic devices. The nanocrystal surface ligands play a crucial role in the transport of photogenerated carriers and ultimately affect the overall performance of PQD solar cells. Significantly improved $CsPbI_3$ PQD synthetic yield and solar-cell performance through surface ligand management are demonstrated. The treatment of a secondary amine, di-*n*-propylamine (DPA), provides a mild and efficient approach to control the surface ligand density of PQDs, which has an apparently different working mechanism compared to previously reported surface treatments. Using an optimal DPA concentration, the treatment can simultaneously remove both long-chain insulating surface ligands of oleic acid and oleylamine, even for unpurified PQDs with high ligand density. As a result, the electrical coupling between PQDs is enhanced, leading to improved charge transport, reduced carrier recombination, and a high power conversion efficiency approaching 15% for $CsPbI_3$-PQD-based solar cells. In addition, the production yield of $CsPbI_3$ PQDs can be increased by a factor of 8. These results highlight the importance of developing new ligand-management strategies, specifically for emerging PQDs to achieve scalable and high-performance perovskite-based optoelectronic devices.**

All-inorganic perovskite quantum dots (PQDs) exhibit high photoluminescence quantum yields, spectrally tunable bandgap, flexible compositional control, and crystalline strain benefits.[1–4] PQDs are relatively easy to synthesize which opens a route for next-generation optoelectronic devices, as well as opportunities for exploring fundamental properties at nanoscale.[5,6] For photovoltaics (PVs), colloidal $CsPbI_3$ PQD solar cells were first demonstrated with a power conversion efficiency (PCE) exceeding 10% and showed improved perovskite phase stability over bulk thin-film $CsPbI_3$,[7] which will convert to a non-perovskite orthorhombic phase ($\delta$-phase) with unfavorable optoelectronic properties at room temperature.[8–10] Now several $CsPbI_3$-PQD-based solar cells show PCEs over 13%,[11–14] with a high open-circuit voltage ($V_{oc}$) up to 1.3 V, and the latest certified record efficiency of 16.6% for QD solar cells has been achieved using $Cs_{0.5}FA_{0.5}PbI_3$ composition.[15] However, the performance of $CsPbI_3$ PQD solar cell still lags behind that of thin-film-based devices,[16,17] mainly limited by the relatively low short-circuit current density ($J_{sc}$) due to inefficient carrier transport. It is reported that the carrier transport in the QD array is largely determined by the ligand management on the QD surface.[18] QDs synthesized by hot-injection method are usually capped by ligands with long alkyl chains, which have to be partially removed to achieve desired charge transport.[19] Methyl acetate (MeOAc) is widely used as an anti-solvent to purify $CsPbI_3$ PQDs and reduce the surface bound oleate ligands.[20] The density of surface ligands is critical, which governs the balance between carrier transport and PQD phase stability. Dense ligands will certainly hinder inter-dots charge hopping, while too few ligands will not allow phase stabilization of the cubic $CsPbI_3$ PQDs. In addition, the chemical bonding between ligands and $CsPbI_3$ PQDs is intrinsically much more ionic. Ligand exchange strategies developed in lead chalcogenides QDs are too strong and normally induce unexpected decomposition of $CsPbI_3$ PQDs.[21–23] Thus it requires strategies to manage the surface ligands of $CsPbI_3$ PQDs with a mild process and achieve optimal photovoltaic performance. Wheeler et al. recently reported that formamidinium iodide (FAI) salt can remove oleylammonium ligands on the surface of $CsPbI_3$ PQD by cation exchange, and speculated that MeOAc can hydrolyze to acetic acid and methanol to remove oleic acid

Y. Wang, Prof. J. Yuan, X. Zhang, X. Ling, Y. Shi, Prof. W. Ma
Institute of Functional Nano & Soft Materials (FUNSOM)
Jiangsu Key Laboratory for Carbon-Based Functional Materials & Devices
Joint International Research Laboratory of Carbon-Based Functional Materials and Devices
Soochow University
199 Ren-Ai Road, Suzhou Industrial Park, Suzhou 215123, P. R. China
E-mail: jyyuan@suda.edu.cn; wlma@suda.edu.cn

Dr. B. W. Larson, Dr. Q. Zhao, Dr. J. M. Luther
Chemistry and Nanoscience Department
National Renewable Energy Laboratory
Golden, CO 80401, USA

Dr. Y. Yang
Shanghai Synchrotron Radiation Facility
Shanghai Institute of Applied Physics
Chinese Academy of Sciences
Shanghai 201204, P. R. China

The ORCID identification number(s) for the author(s) of this article can be found under https://doi.org/10.1002/adma.202000449.

**DOI: 10.1002/adma.202000449**

 © 2020 WILEY-VCH Verlag GmbH & Co. KGaA, Weinheim

ligand on the surface of $CsPbI_3$ PQD by anion exchange.[20] However, the hydrolysis of MeOAc is slow without the aid of acids and bases, which will certainly limit the removal of oleic acid ligand. Therefore, it is of great significance to develop a more efficient approach with different working mechanisms to remove the native ligands for further improving the carrier transport in $CsPbI_3$ PQD solar cells.

In this contribution, we developed an effective way to control the surface ligand density of $CsPbI_3$ PQDs with the aid of a secondary amine, di-*n*-propylamine (DPA), which allows a mild process to prevent damage to the treated PQDs. We characterized the structural, optical, electrical, and morphological properties of the resultant $CsPbI_3$ PQD films and reveal that DPA treatment can simultaneously enable efficient ligand removal and maintain the integrity of $CsPbI_3$ PQDs. As a result of enhanced electrical coupling, the solar cell efficiency is improved to ≈15.0%. More importantly, the DPA process has the potential to reduce the PQD purification steps, and thus increases the synthetic yield of PQDs for the realization of improved scalability of PQD solar cells in the future.

**Figure 1**a illustrates the synthesis and purification steps of $CsPbI_3$ PQDs. In specific, the $CsPbI_3$ PQDs are normally synthesized in a nitrogen gas atmosphere via a classical hot-injection method using $PbI_2$ dissolved in oleic acid (OA), oleylamine (OLA), and 1-octadecene (ODE) at elevated temperature. Cs-oleate is injected to initiate the reaction and form $CsPbI_3$ PQDs as described in previous work.[12,13] In step I, the as-synthesized PQDs are precipitated by adding MeOAc to the reaction mixture and then centrifuged. In order to further remove more ligands and unreacted precursors, in step II, the as-synthesized $CsPbI_3$ PQDs are completely dispersed in hexane and precipitated again with an equal volume of MeOAc and centrifuged. It should be noted that the addition of MeOAc during step II causes a significant amount of the PQDs to agglomerate due to the excessive removal of ligands. As a result, the PQDs precipitates of step II can only be partially redispersed in hexane. The undissolved solids have to be

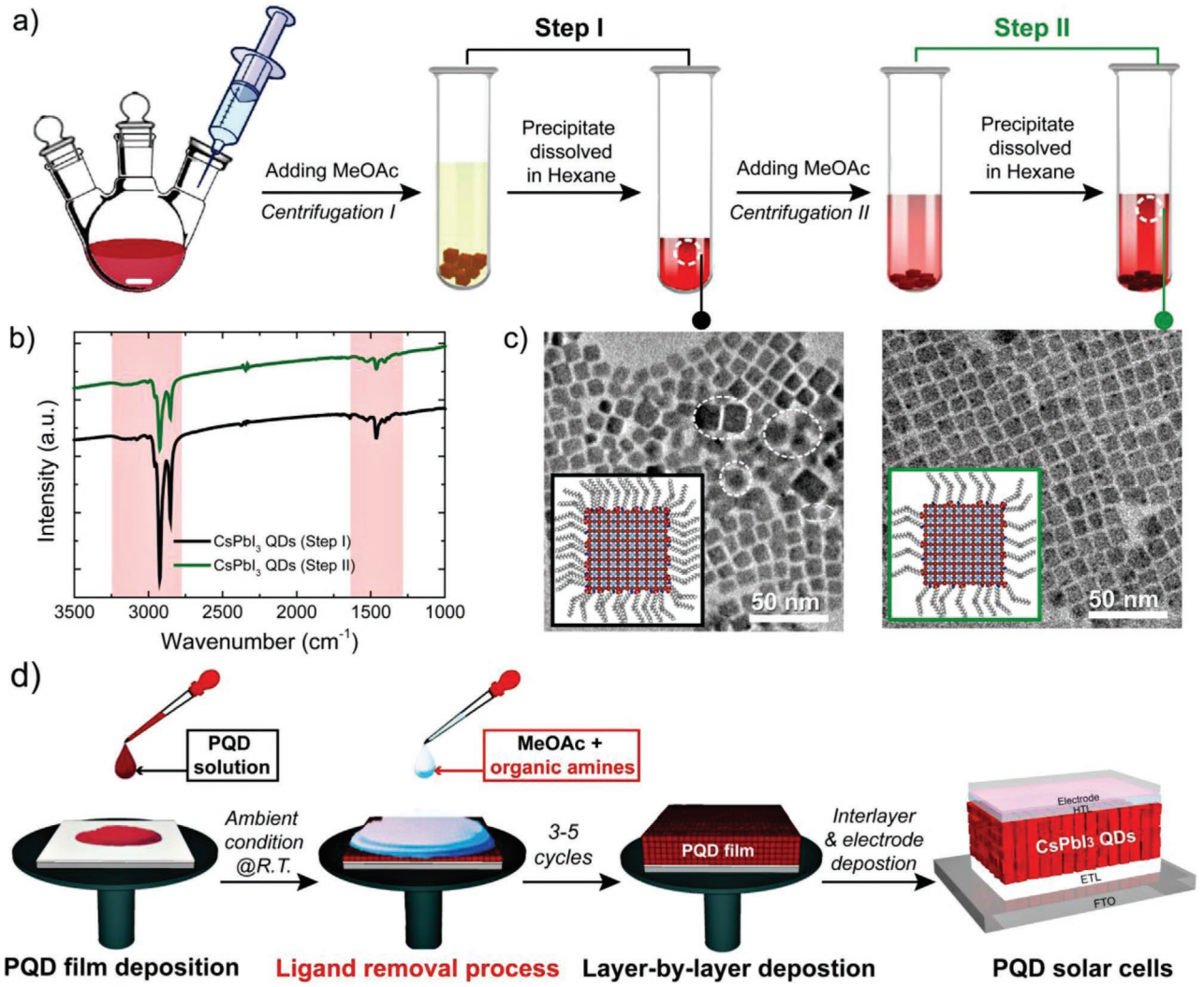


**Figure 1.** a) The preparation and purification process of $CsPbI_3$ PQDs. b) FTIR spectra of the $CsPbI_3$ PQD films based on the step I purified and step II purified $CsPbI_3$ PQDs. c) TEM images of the step I purified and step II purified $CsPbI_3$ PQDs. d) Schematic diagram of the fabrication of $CsPbI_3$ QD solar cells.


© 2020 WILEY-VCH Verlag GmbH & Co. KGaA, Weinheim

removed, thus reducing the production yield. Hexane is evaporated through a rotary evaporator and the obtained PQD solids are finally dispersed in octane at a concentration of 70 mg $mL^{-1}$ for solar cell fabrication. We calculated that the product yield after step II is eight times lower than that after step I ($PbI_2$: 1 g, $CsPbI_3$ PQD: step I: 400 mg; step II: 50 mg) due to the agglomeration. $CsPbI_3$ PQDs (70 mg $mL^{-1}$) after step I or step II purification were spun on the $CaF_2$ substrates for Fourier transform infrared (FTIR) characterization. As shown in Figure 1b, the FTIR results reveal significantly higher surface ligand density for PQDs with a single purification (after step I) compared with double purified PQDs (after step II), indicating the effect of ligand removal by using MeOAc. Bands at 3138 $cm^{-1}$ are assigned to the stretching vibration of $NH^{3+}$ group, originating from OLA.[19] Features at 2768–2986 $cm^{-1}$ ($C-H_x$), 3005 $cm^{-1}$ (C=C−H) and 1462 $cm^{-1}$ ($C-H_2$) are derived from the oleyl groups on OA and OLA ligands.[24] 1404 and 1524 $cm^{-1}$ correspond to the symmetric and asymmetric stretching vibrations of $COO^-$ group, originating from OA.[25,26] Transmission electron microscopy (TEM) was used to investigate the size distribution of the PQDs prepared in each step. As shown in Figure 1c (with lower magnification images shown in Figure S1, Supporting Information), after step II purification, the $CsPbI_3$ PQDs exhibit higher uniformity in size and shape with an average size around 9 nm, compared to the step I PQDs. However, despite of dense surface ligands and wide size distribution, the step I PQDs have a significantly higher synthetic yield without the extra MeOAc washing, beneficial for scalable application.

Figure 1d shows a schematic illustration of the $CsPbI_3$ PQD solar cell fabrication process using the conventional layer-by-layer methodology. After deposition of each PQD film, neat MeOAc or MeOAc with different organic amines is applied to remove QDs surface ligands. The $CsPbI_3$ PQD solar cells were fabricated with a planar structure of glass/fluorine-doped tin oxide (FTO)/$TiO_2$ (40 nm)/$CsPbI_3$ PQDs (500 nm)/poly(triarylamine) (PTAA, 60 nm)/$MoO_3$ (8 nm)/Ag (120 nm), and the device structure is clearly identified in the cross-sectional scanning electron microscopy (SEM) image (**Figure 2**a). The thick active layer is fabricated by five depositions of thin layers (≈100 nm). As shown in Figure 2b and Table S1, Supporting Information, solar cells processed with a series of organic amines, were investigated to study the structural effect of organic amines on device performance and screen the best post-treatment. It is evident that the secondary amine outperforms their primary and tertiary counterparts with the same length of aliphatic chain (DPA vs *n*-butylamine [NBA] and tri-*n*-propylamine [TPA]). We observe that further increasing the length of aliphatic chain leads to decreased solar cell performance for both primary and secondary amines. Meanwhile, treatment using organic aromatic amine like phenylamine (NPhA) and diphenylaniline (DPhA) exhibit similar effect compared to neat MeOAc treatment, less effective than organic aliphatic amines. Resultantly, the $CsPbI_3$ PQD solar cells treated by MeOAc with secondary amines DPA exhibit the best device performance. And DPA treatment was used to study the subsequent QDs surface ligand change. Figure 2c,d presents the current density versus voltage (*J*–*V*) characteristics of the optimal solar cells using different $CsPbI_3$ PQDs, under AM 1.5G illumination at an intensity of 100 mW $cm^{-2}$, with the device parameters shown in **Table 1**. Considering the significantly lower material cost of step I $CsPbI_3$ PQDs, we first investigated their PV performance and compared it with step II PQDs with better size distribution but much less final production yield. The solar cells exhibit best PCEs of 5.4% and 13.2% for step I PQDs and step II PQDs respectively. Specifically, for step I PQDs with a high ligand density, depositing an additional PQD layer partially removes the underlying layers due to redissolution (confirmed by the film image insert in Figure 2c). Therefore, a poor PCE of 5.4% is obtained with a low $J_{sc}$ of 7.39 mA $cm^{-2}$. In comparison, the MeOAc treatment can further remove the native ligands and allow upper layers to be deposited without redissolving underlying layers using step II purified QDs (confirmed by the film image insert in Figure 2d). After optimizing the thickness of the PQD film, a best PCE of 13.2% is achieved with significantly improved $J_{sc}$ and fill factor (FF) due to enhanced electrical coupling and carrier transport. By adding DPA to MeOAc, after optimizing the DPA content (Table S2, Supporting Information), the performance of devices based on step I and II PQDs are both improved. To demonstrate how effective DPA is on further ligand removal, we treat the step I PQDs film with DPA, the previous issue of redissolution is resolved, suggesting that DPA removes far more ligands than neat MeOAc and allows the PQDs with less purification steps to achieve decent PV performance. As shown in Figure 2c and Table 1, after DPA treatment, a significantly enhanced PCE up to 11.2% is obtained for step I PQDs with a higher $J_{sc}$ of 12.26 mA $cm^{-2}$ and a higher FF of 74.54%. For step II PQDs, the efficiency is further improved to 14.9%, due to simultaneous increases in $V_{oc}$ (1.243 V), $J_{sc}$ (15.84 mA $cm^{-2}$), and FF (75.50%). The PCE distributions of 20 devices for each case are shown in Figure 2e, validating the performance enhancement of the device. Additionally, the DPA treatment can significantly improve the device reproducibility. However, we did not witness any significant improvement of device storage stability under ambient conditions (Figures S2 and S3, Supporting Information). It is worth noting that even for the step II $CsPbI_3$ PQDs, as shown in Figure S4, Supporting Information, they sometimes have batch-to-batch variation in surface ligands density, which could bring the same film redissolution issue as we witnessed for step I PQDs. The resultant $CsPbI_3$ PQD solar cells therefore exhibit a low efficiency. Fortunately, DPA:MeOAc treatment improves the film quality and pushes the PCE to steadily over 14%. In Figure S5, Supporting Information, we show the external quantum efficiencies (EQEs) of optimized devices treated by MeOAc with/without w/wo DPA and the corresponding integrated $J_{sc}$ values are 15.25 mA $cm^{-2}$ (15.84 mA $cm^{-2}$ from *J*–*V* curve) and 14.03 mA $cm^{-2}$ (14.42 mA $cm^{-2}$ from *J*–*V* curve), respectively, which is within 5% error compared to the corresponding $J_{sc}$ obtained from the *J*–*V* curves. We observe enhanced EQE across the entire response region, which can be attributed to simply better charge transport by DPA treatment.[27] We also characterized hysteresis (Figure S6, Supporting Information), and found almost negligible hysteresis for both devices.[28] Figure S7, Supporting Information, shows the stabilized power output of the devices using DPA:MeOAc treatment by measuring the PCE at the maximum power


© 2020 WILEY-VCH Verlag GmbH & Co. KGaA, Weinheim

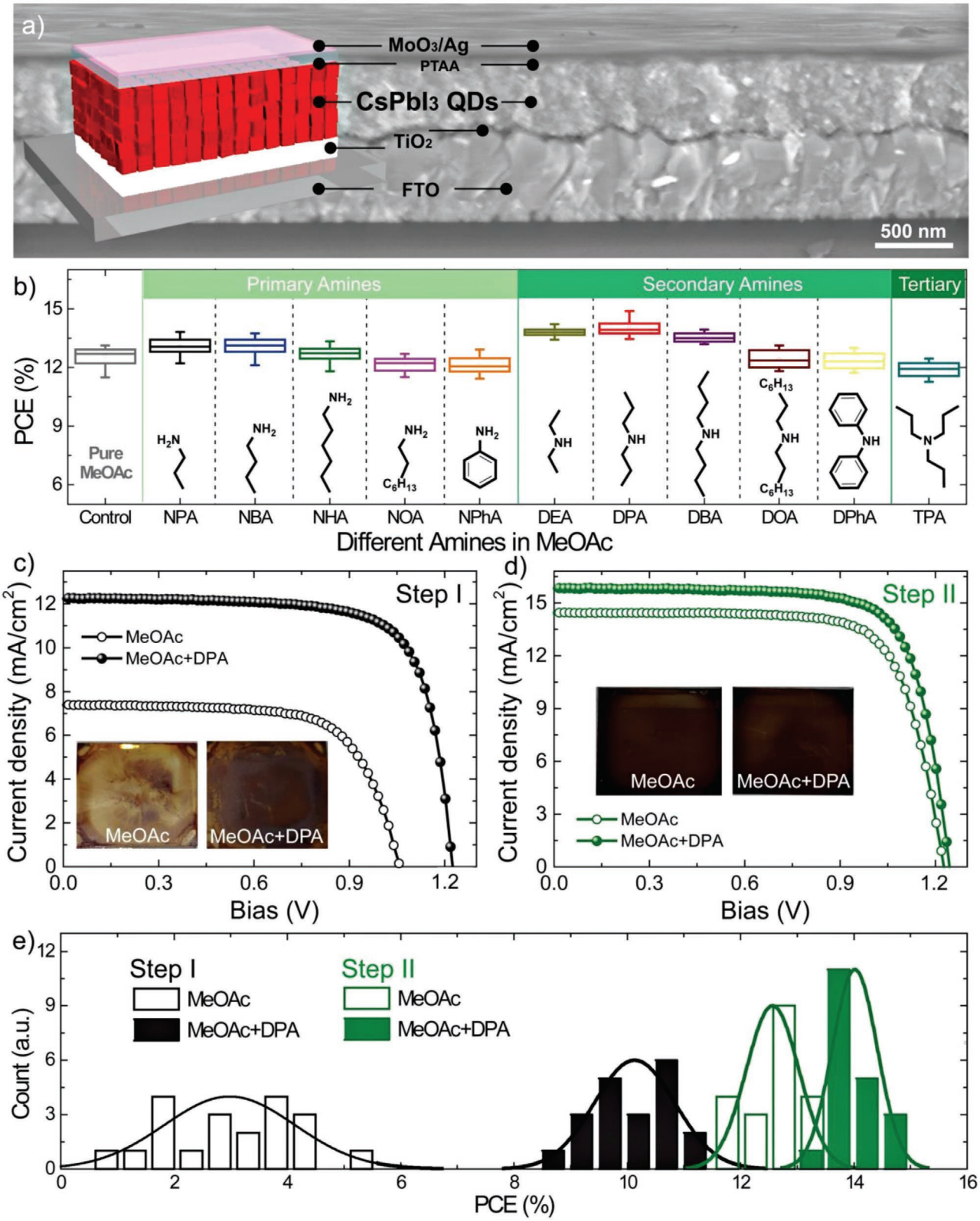


**Figure 2.** a) Illustration and cross-sectional SEM image of the $CsPbI_3$ PQD solar cell. b) PCEs of $CsPbI_3$ QD solar cells as a function of QD film post-treatment method. c,d) Current–voltage characteristics of the $CsPbI_3$ PQD solar cells based on the step I purified (c) and step II purified (d) $CsPbI_3$ PQDs treated by MeOAc w/wo DPA; the inset shows the $CsPbI_3$ PQD films treated by MeOAc w/wo DPA. e) Histograms of PCEs for the $CsPbI_3$ PQD solar cells based on the step I purified and step II purified $CsPbI_3$ PQDs treated by MeOAc w/wo DPA.

 © 2020 WILEY-VCH Verlag GmbH & Co. KGaA, Weinheim

**Table 1.** Device parameters of the $CsPbI_3$ PQD solar cells based on the as-synthesized and purified $CsPbI_3$ PQDs treated by MeOAc w/wo DPA, the average values were summarized from 20 parallel devices for each condition.

| Purification | Post-treating | $V_{oc}$ [V] | $J_{sc}$ [mA cm$^{-2}$] | FF [%] | PCE [%] |
|---|---|---|---|---|---|
| Step I | MeOAc | 0.931 ± 0.140 | 4.86 ± 0.53 | 60.16 ± 8.34 | 3.1 ± 2.3 |
| | Champion | 1.060 | 7.39 | 68.49 | 5.4 |
| | MeOAc+DPA | 1.212 ± 0.009 | 11.92 ± 0.34 | 69.00 ± 5.54 | 10.2 ± 1.3 |
| | Champion | 1.221 | 12.26 | 74.54 | 11.2 |
| Step II | MeOAc | 1.213 ± 0.024 | 13.70 ± 0.72 | 74.09 ± 0.52 | 12.6 ± 1.1 |
| | Champion | 1.222 | 14.42 | 74.60 | 13.2 |
| | MeOAc+DPA | 1.228 ± 0.025 | 15.31 ± 0.53 | 75.06 ± 0.89 | 14.0 ± 0.9 |
| | Champion | 1.243 | 15.84 | 75.50 | 14.9 |

point. The cells exhibit steady power output (SPO) values of 14.5%, confirming the reliability of PCE obtained from the $J$–$V$ measurements.

In order to further understand the device improvement, more characterization techniques were performed on $CsPbI_3$ PQD solar cells. Figures S8 and S9, Supporting Information, present the $J_{sc}$ and $V_{oc}$ measurements as a function of illumination intensity. Figure S8, Supporting Information, shows the values of the exponential factor ($\alpha$) as 0.98 and 0.99 for the devices w/wo DPA treatment, respectively. The $J_{sc}$ is expected to demonstrate a power-law dependence with light intensity $I$ ($J_{sc} \propto I^{\alpha}$). This result indicates that DPA addition has a negligible impact on bimolecular recombination.[13] Moreover, the light intensity dependence on $V_{oc}$ was also studied. If the slope is greater than 1.0 $kT/q$ (where $k$ is the Boltzmann constant, $T$ is the temperature, and $q$ is the elementary charge), it indicates trap-assisted Shockley–Read–Hall (SRH) recombination. The values of the slope were calculated to be 1.41 $kT/q$ and 1.65 $kT/q$ for the devices w/wo DPA treatment, respectively. This suggests a reduction in trap-assisted carrier recombination, which is typically the dominant recombination mechanism in these PQD solar cells,[29,30] for the devices with DPA treatment. Electrochemical impedance spectroscopy (EIS) was used to investigate charge transfer and carrier recombination within the device stack. Figure S10, Supporting Information, shows Nyquist plots of the devices treated by neat MeOAc and DPA:MeOAc. Analysis of the low-frequency region, including recombination chemical capacitance ($C_{rec}$) and the recombination resistance ($R_{rec}$), provides insight into the recombination processes at play, whereas analysis of the high-frequency region, including transport chemical capacitance ($C_{trans}$) and the transport resistance ($R_{trans}$), gives information about the charge transport processes.[31] The corresponding parameters from theses analyses are listed in Table S3, Supporting Information, showing that the device with DPA:MeOAc treatment presents smaller $R_{trans}$ and larger $R_{rec}$ than the one with neat MeOAc treatment, indicating that the recombination process is effectively suppressed, consistent with our light intensity measurements on the devices.

The performance of PV devices depends critically on charge carrier transport properties. To probe the impact of DPA:MeOAC on the carrier dynamics of $CsPbI_3$ PQDs, we performed steady-state photoluminescence (PL), time-resolved photoluminescence (TRPL), and time-resolved microwave conductivity (TRMC) measurements. **Figure 3**a displays PL spectrum of the $CsPbI_3$ PQD films treated by MeOAc w/wo DPA. The PL emission peaks red-shift from 697 to 707 nm with DPA, suggesting enhanced coupling between $CsPbI_3$ PQDs as a result of less ligand density. The TRPL spectra exhibit the same general trend and the average lifetime is improved from 2.4 to 4.5 ns with DPA treatment, as shown in Figure 3b and Table S4, Supporting Information. To examine the impact of DPA on the mobility of photoinduced charges in our $CsPbI_3$ PQDs, we performedTRMC measurements, a technique that measures the attenuation of a GHz frequency microwave probe beam by mobile charge carriers.[32] The TRMC figure of merit ($\phi\Sigma\mu$) arises from the product of the quantum yield of free charge carrier generation by a 5 ns laser pulse per photon absorbed ($\phi$) and the summation of the electron and hole mobilities ($\Sigma\mu$).[33] Figure 3c shows the TRMC yield–mobility product of PQDs w/wo DPA treatment. The $CsPbI_3$ PQD film treated by DPA:MeOAC shows a yield–mobility product of 0.774 cm$^2$ V$^{-1}$ s$^{-1}$, higher than the one treated by pure MeOAc (0.412 cm$^2$ V$^{-1}$ s$^{-1}$). Bi-exponential fits of the photoconductivity transient over 500 ns, as shown in Figure S11, Supporting Information, reveal that the average free carrier lifetime is also higher in the DPA:MeOAc treated PQD film, in agreement with reduced carrier recombination. With the experimentally determined yield–mobility product ($\mu$) and carrier lifetime ($\tau$) at GHz frequencies, we can further evaluate the free charge carrier diffusion length ($L_D$) using the following equation:

$$L_D = \sqrt{\tau \frac{\mu k_B T}{q}} \tag{1}$$

where $\tau$, $\mu$, $k_B$, $T$, and $q$ are charge carrier lifetime, charge mobility, Boltzmann constant, temperature, and elementary charge, respectively.[11,13,33,34] As shown in Figure 3d, the DPA:MeOAc treated film exhibits a significantly higher free carrier diffusion length ($L_D$ = 636 nm) relative to the MeOAc treated one ($L_D$ = 407 nm) at an assumed internal quantum yield of 1, as well as over a full range of simulated yield values from 0.4 to 1.0. These results indicate the intrinsic carrier properties (within grain) of the PQD film after solid-state post-treatment with DPA:MeOAc is significantly enhanced compared to treatment with MeOAc only.

Meanwhile, the effects of DPA on surface morphology and crystal structure properties of $CsPbI_3$ PQD film were also


© 2020 WILEY-VCH Verlag GmbH & Co. KGaA, Weinheim

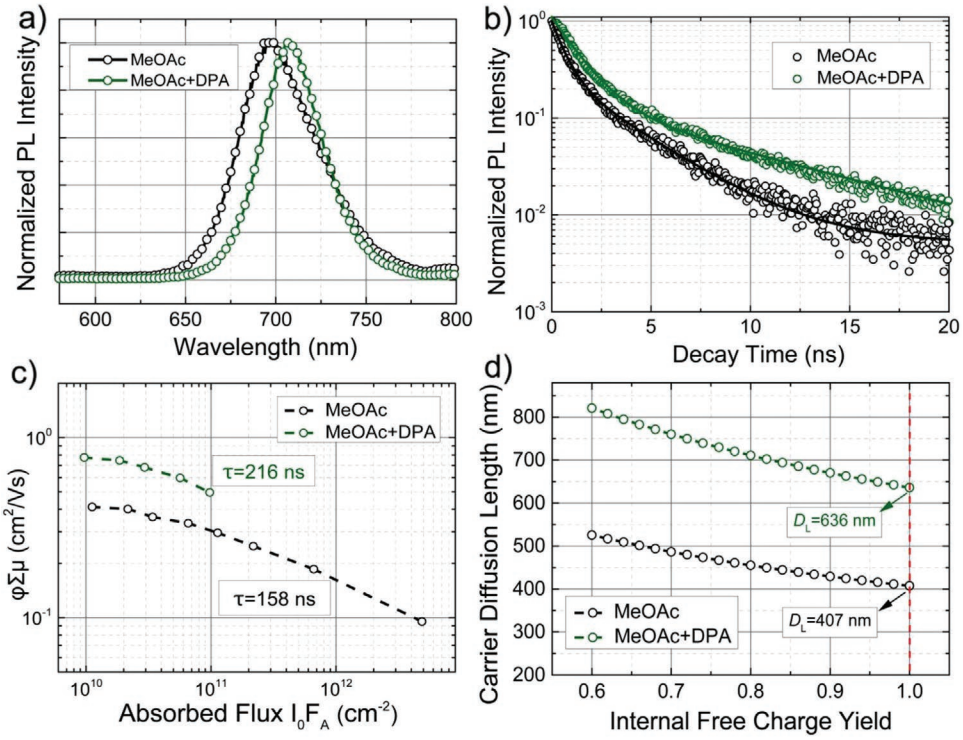


**Figure 3.** a) Steady state and b) transient PL spectra of the $CsPbI_3$ PQD films treated by MeOAc w/wo DPA. c) The product of charge carrier yield ($\varphi$) and sum of hole and electron mobilities ($\Sigma\mu$), and d) free carrier diffusion length of the $CsPbI_3$ PQD films treated by MeOAc w/wo DPA excited at a laser wavelength of 640 nm in TRMC measurements.

investigated. The top-view SEM images in **Figure 4**a,b clearly show that the DPA:MeOAc treatment apparently produces a denser PQD film with significantly reduced pin-holes. A similar trend is also found in the atomic force microscopy (AFM) height images (Figure 4c,d). The DPA:MeOAc treated film shows a smoother surface (RMS: 7.0 nm) morphology compared

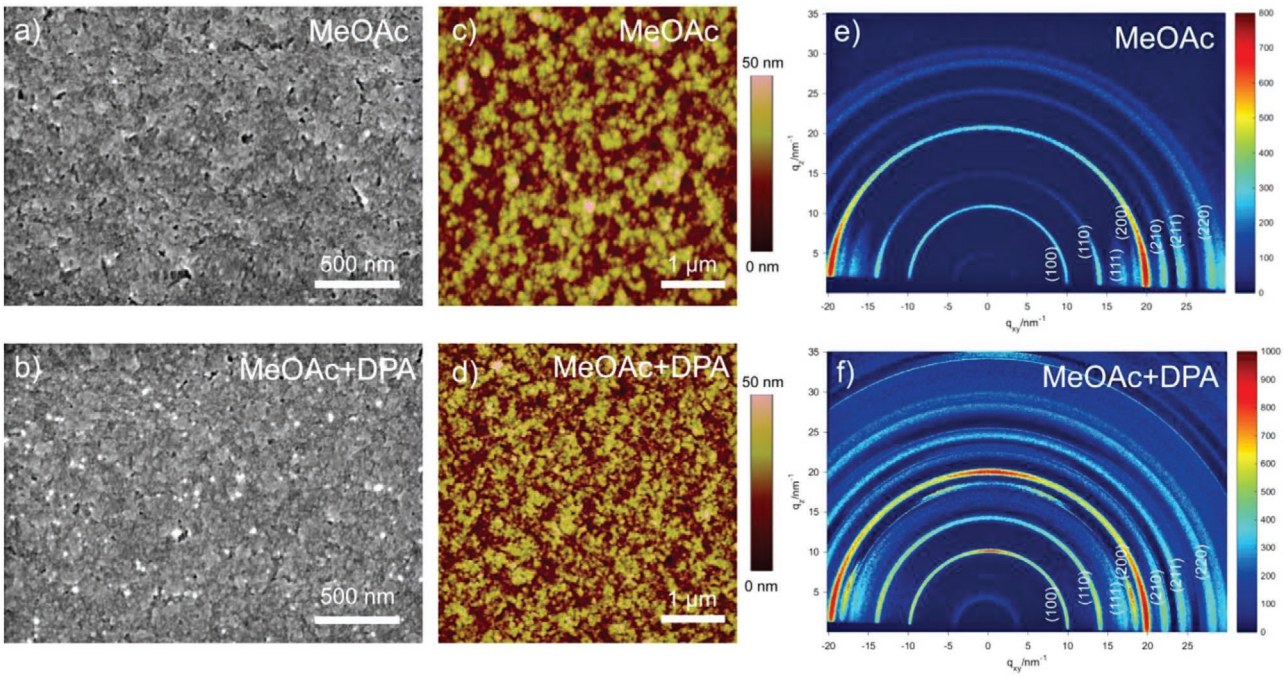


**Figure 4.** a,b) The top-view SEM, c,d) AFM height images, and e,f) 2D-GIWAXS patterns of $CsPbI_3$ PQD films treated by neat MeOAc and DPA+MeOAc.


© 2020 WILEY-VCH Verlag GmbH & Co. KGaA, Weinheim

to the neat MeOAc treated one (RMS: 8.3 nm), which may be attributed to the closely packed assemblies of $CsPbI_3$ PQDs with less bulky surface ligands. Then, the crystalline nature of $CsPbI_3$ PQDs in the as-prepared $CsPbI_3$ PQD film was evaluated by synchrotron-based 2D grazing-incidence wide-angle X-ray scattering (GIWAXS) as shown in Figure 4e,f.[35] Both samples exhibit strong X-ray characteristic diffractions of PQDs.[4] We observe apparent diffraction peaks of (100), (110), (111), (200), (210), (211), and (220) at preferable positions for the $CsPbI_3$ PQD film w/wo DPA, indicating high crystallinity and a preferable orthogonal orientation relative to the substrate. For the DPA:MeOAc treated PQD film, a significantly enhanced peak intensity along the out-of-plane ($q_z$) axis can be observed and the intensity of nearly all the diffraction peaks along the in-plane ($q_{xy}$) axis is also enhanced. These results indicate that enhanced coupling between PQDs and multiple-order in the packing orientations of PQDs are achieved, likely attributed to the reduced ligand density through DPA treatment, which would result in efficient charge transport along multiple directions.[36]

Finally, in order to gain more insight into the underlying chemical reactions and surface chemistry during ligand removal process assisted by DPA, we again conducted FTIR characterization as well as nuclear magnetic resonance (NMR) measurement on the PQDs. **Figure 5**a shows the FTIR spectra of step II $CsPbI_3$ PQD pellets w/o MeOAc treatment, with neat MeOAc treatment, with MeOAc:DPA(low content) and MeOAc:DPA (high content) treatment. The FTIR spectrum of the untreated PQDs is dominated by vibrational modes of bound and unbound ligand molecules: oleyl group ($\nu$(C–$H_x$) = 2768–2986 $cm^{-1}$, $\nu$(C=C–H) = 3005 $cm^{-1}$, and $\nu$(C–$H_2$) = 1462 $cm^{-1}$), a broad resonance centered at 3138 $cm^{-1}$ due to stretching vibrations of N–$H_3^+$ group, and the resonances centered at 1404 and 1524 $cm^{-1}$ correspond to the symmetric and asymmetric stretching vibrations of $COO^-$ group. The relative intensity of the FTIR characteristic peaks significantly decreases for samples treated with neat MeOAc, indicating the bulky long organic ligands are partially removed. Wheeler et al. indicated that MeOAc mainly play the role of removing OA ligands by the hydrolysis of MeOAc to produce acetate ion in the presence of humidity.[20] However, we conducted the experiment inside a dry air box, suggesting that the hydrolysis of MeOAc is difficult under regular condition. Hence, the FTIR peaks of $COO^-$ group are from OA ligands, indicating substantial remaining surface bound OA ligands even after neat MeOAc treatment. Adding a small amount of DPA can further decrease the peak intensity, and we find characteristic FTIR peaks are almost completely eliminated when increasing the DPA concentration in MeOAc. Thus we concluded that both OLA and OA ligands

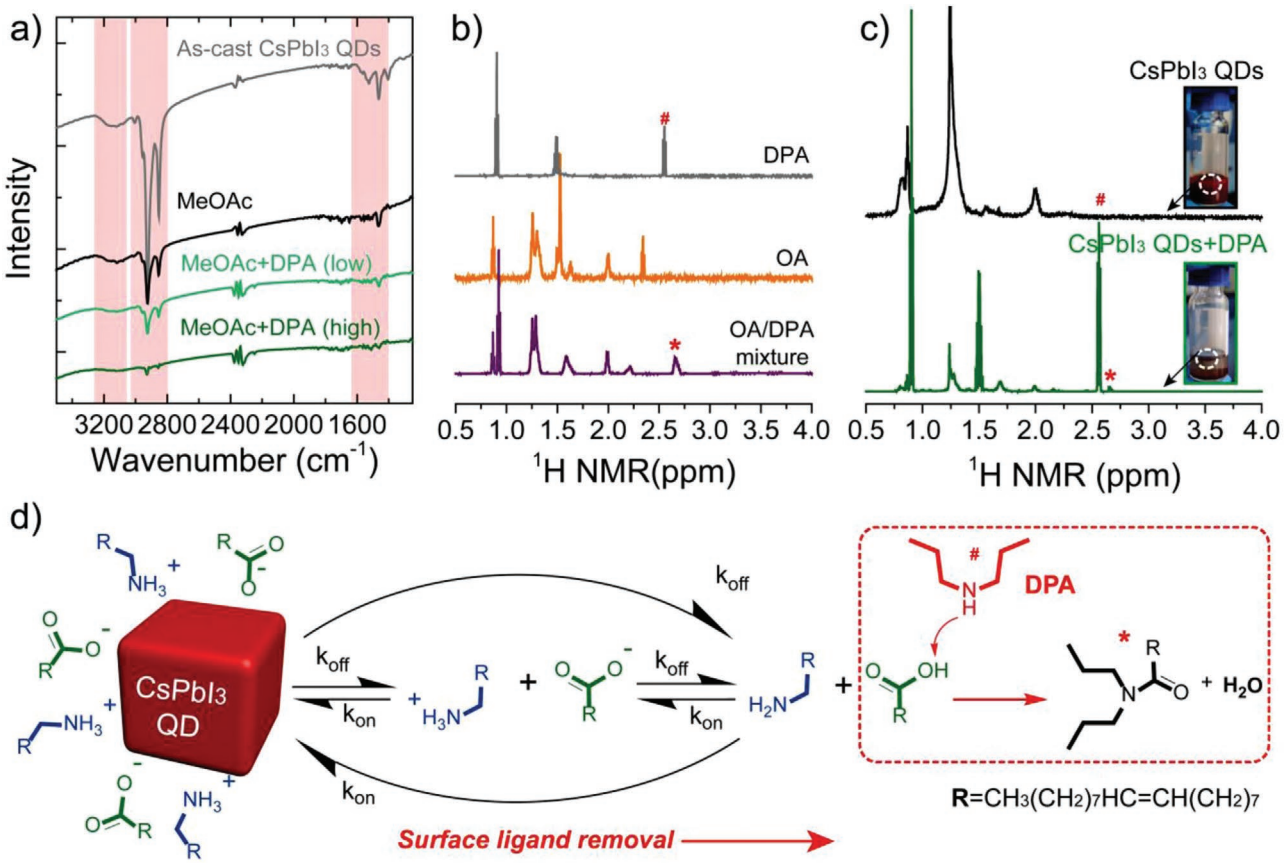


**Figure 5.** a) FTIR spectra of the $CsPbI_3$ PQD films with varying post-treatment condition (low: DPA/MeOAc v/v = 0.5/3000, high: DPA/MeOAc v/v = 2/3000). b) $^1$H NMR spectra of DPA, OA, and the mixture of OA and DPA with a molar ratio of 1:1. c) $^1$H NMR of $CsPbI_3$ PQDs solution and the liquid supernatant by adding excess DPA to $CsPbI_3$ PQDs solution. d) Schematic representation of the PQD dynamic surface stabilization and the ligand removal process assisted by DPA.


© 2020 WILEY-VCH Verlag GmbH & Co. KGaA, Weinheim

can be efficiently removed by the DPA treatment with optimal concentration. To reveal the surface chemical reactions by the introduction of DPA, we first conducted $^1$H NMR characterization on OA, DPA, and DPA/OA mixture (molar ratio = 1/1). $^1$H NMR in particular has the possibility to go beyond the structure analysis of organic compounds in solution and can effectively probe the dynamics of chemical reactions. We planned to verify the possible reactions that might involve DPA. At first, there should be no chemical reaction between DPA and OLA, since they are both alkylamines. For DPA and OA, as shown in Figure 5b, we probe the chemical shift of methylene (denoted by #, 2.55 ppm) next to the secondary amines group in DPA and it shifts to 2.67 ppm (denoted by *) by adding equal amount of DPA to OA, indicating a quantitative chemical reaction between DPA and OA. To confirm, the step II $CsPbI_3$ PQD solution and the liquid supernatant of $CsPbI_3$ PQD solution after adding excessive DPA (Note that adding excess DPA appears to remove the surface ligands, causing the PQDs to agglomerate) were also tested and collected by $^1$H NMR spectrum (Figure 5c). In the spectrum of the supernatant, we observe strong characteristic resonances at 2.55 ppm from methylene next to the secondary amines group of excess DPA. Again, we also observe the characteristic resonances at 2.67 ppm, which indicates the same reaction product found in previously investigated DPA/OA mixture. Thus we confirm that chemical reaction will occur between DPA and OA ligands at the surface of $CsPbI_3$ PQDs.

Since typical ligand binding to PQDs is highly labile in nature, ligands are easily lost during the isolation and purification procedures. Figure 5d shows a schematic representation of the dynamic surface stabilization by $R{-}CH_2{-}NH_3^+$ and $R{-}COO^-$ native ligands. The behavior of these native ligands is dynamic thus produce free $R{-}CH_2{-}NH_3^+$ and $R{-}COO^-$ ions at solution state and achieve dynamic equilibrium with bonding ligands attached to the PQD surface. Meanwhile, the free $R{-}CH_2{-}NH_3^+$ and $R{-}COO^-$ ions could achieve another chemical equilibrium with pure OA and OLA, which has been confirmed in the $CsPbBr_3$ PQD system.[37] Our XPS results (Figure S12, Supporting Information) show that both $Cs^+/I^-$ and $Pb^{2+}/I^-$ in the PQD film is significantly below the theoretical stoichiometric ratio of 1/3, indicating the presence of excess $I^-$ on the surface. It should be noted here the $I^-$ ion at the PQD surface would generate another dynamic equilibrium: $R{-}CH_2{-}NH_3^+ + I^- = R{-}CH_2{-}NH_2 + HI$. Therefore, the $CsPbI_3$ PQDs surface is stabilized by multiple dynamic bonding equilibria including $R{-}CH_2{-}NH_3^+\ I^-$, $R{-}CH_2{-}NH_3^+$, $R{-}COO^-$, OA and OLA. The addition of DPA into MeOAc during the solid-state treatment will induce acylation reaction between DPA and OA. As shown in the following reaction scheme:

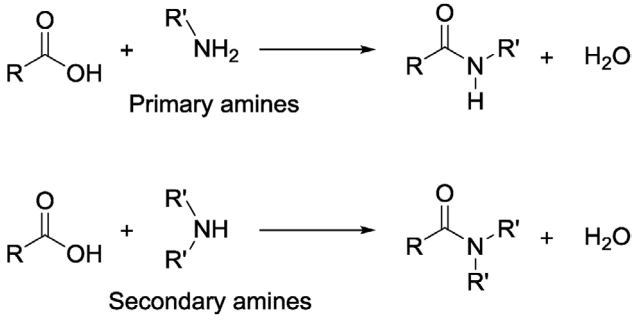


Acylation reaction normally happens between amino and carboxyl group (at molar ratio of 1/1) depending on the reactivity of both groups. OA is a weak organic acid, and it needs relatively strong organic amine for efficient acylation reaction. According to the $^1$H NMR results, DPA can react with OA without any additional heating treatment, and the reaction formula of DPA and OA is shown in the dashed box in Figure 5d. The acylation reaction hence will quickly consume the dissociative OA and shift the whole reaction toward the right direction, resulting in efficient removal of both $R{-}CH_2{-}NH_3^+$ and $R{-}COO^-$ ligands attached to the $CsPbI_3$ PQD surface (Figure 5d). Because of this complex and dynamic ligand binding scheme, we propose that the native ligand removal process should be performed under optimal DPA concentrations for mild reactions since excessive DPA concentration in MeOAc quickly shifts the equilibrium toward fewer bound ligands. This effect, in turn, causes the PQDs with lower surface coverage to agglomerate, eventually resulting in a phase-transition or decomposition of these PQDs because of the reduction of surface energy.[38] Hence, the device with excessive DPA treatment presents a higher trap state density to $3.58 \times 10^{11}$ cm$^{-3}$, a lower carrier mobility to 0.376 cm$^2$ V$^{-1}$ s$^{-1}$ (Figure S13, Supporting Information) and decreased phase stability (Figure S14, Supporting Information).[39,40] It is worth noting that the reactivity of the acylation reaction between amino group and carboxyl group is largely determined by the chemical alkalinity of these organic amines. It is well-known that the alkalinity of organic aliphatic amine (with the same alky chain length) shows the following trend in solution state: secondary > tertiary > primary > $NH_3$. Among them, tertiary amine will not directly react with OA due to the lack of hydrogen atom on the amino group, confirmed by the relatively low device performance. Note that the structure, number and length of chains surrounding amino group can also affect the molecule reactivity. Electron-donating groups like alkyl chains can increase the density of electron cloud, thereby increasing the reactivity of amino group. Thus secondary amine with double alkyl chains is more reactive than primary amine with a single chain. In contrast, electron-withdrawing groups like phenyl groups are able to decrease the density of electron cloud, eventually impairing the reactivity of amino group. As a result, no performance improvement can be observed for device treated with organic aromatic amine. In addition, alkyl chain with longer length generally increases the steric hindrance, leading to reduced reactivity of the amino group. Hence, secondary amine with an optimal alkyl chain length like DPA is a rational selection for improving the performance of CsPbI3 PQD solar cell (Figure 2b and Tables S1, Supporting Information).

In summary, we have demonstrated significantly improved synthetic yield of $CsPbI_3$ PQDs and enhanced performance of $CsPbI_3$ PQD solar cells by using efficient surface ligand management. The treatment of a secondary amine, DPA, provides a mild and efficient approach to control the surfaces ligand density of PQDs. The DPA additive can react with OA and accelerate ligand removal during the solid-state treatment process, showing an apparently different working mechanism from the previously reported approaches. Using an optimized DPA concentration, the treatment can efficiently remove both long insulating surface ligands of OA and OLA, even for underpurified


© 2020 WILEY-VCH Verlag GmbH & Co. KGaA, Weinheim

PQDs with high ligand density. As a result, the electrical coupling between PQDs is enhanced, leading to improved charge transport, reduced carrier recombination, and a high PCE approaching 15% for $CsPbI_3$-PQD-based solar cells, which is one of the highest PCEs reported for $CsPbI_3$ QD solar cells to date (Table S5, Supporting Information). In addition, the synthetic yield of $CsPbI_3$ PQDs with decent photovoltaic performance can be increased by eight times. Therefore, we believe that our approach will provide insight into future surface ligand management for perovskite nanocrystals, and enable scalable optoelectronic device manufacturing.

## Experimental Section

*Purification of $CsPbI_3$ PQDs*: For step I, 30 mL of MeOAc was added into 10 mL as-prepared $CsPbI_3$ PQD solution and centrifuged at 8000 rpm for 5 min aiming at removing ODE, unreacted OA, and unreacted OLA. The precipitation was redispersed into 3 mL of hexane. For step II, 3 mL of MeOAc was added into 3 mL $CsPbI_3$ PQD hexane solution and centrifuged at 8000 rpm for 3 min aiming at removing undersized $CsPbI_3$ PQDs. Then, all the precipitation was redispersed into 20 mL of hexane and centrifuged at 4000 rpm for 5 min. The last precipitation was not needed aiming at removing excess $PbI_2$, excess Cs-oleate and oversized $CsPbI_3$ PQDs. For the $CsPbI_3$ PQDs through step I or steps I and II together, they needed to be stored in dark at −4 °C overnight and centrifuged at 4000 rpm for 5 min aimed at removing excess $PbI_2$, Cs-oleate, and Pb-oleate to achieve $CsPbI_3$ PQD solid. The $CsPbI_3$ PQD solid was dispersed into octane for 70 mg $mL^{-1}$ to prepare $CsPbI_3$ PQD solar cells.

*Preparation of $CsPbI_3$ PQD Solar Cells*: $TiO_2$ electron transfer layer was deposited on the FTO substrate by means of chemical bath deposition as reported previously.[41] Before depositing $CsPbI_3$ PQDs, the FTO/$TiO_2$ substrates were treated by UV-ozone for about 10 min and transferred to a glove box in which atmosphere was 70% of $N_2$ and 30% of $O_2$. Then, 15 µL of as-prepared octane solution of $CsPbI_3$ PQDs was spin-coated on the FTO/$TiO_2$ substrate at 1000 rpm for 15 s and 2000 rpm for 20 s. 150 uL of MeOAc containing or not containing DPA was dropped on the $CsPbI_3$ PQD layer for 5 s to remove the long chain insulated ligands at the surface of $CsPbI_3$ PQD and then spun at 2000 rpm for 20 s. This process was needed to repeat five times to obtain thick enough $CsPbI_3$ CQD film. The film was soaked into saturated solution of ethyl acetate of FAI and pure MeOAc for 3 s, respectively, and then blown dry with $N_2$. The as-prepared substrate was transferred to a glove box with pure $N_2$ to deposited hole transfer layer. 15 mg $mL^{-1}$ of tris(pentafluorophenyl) borane-doped PTAA toluene solution was spin-coated on the as-prepared FTO/$TiO_2$/$CsPbI_3$ PQDs substrate at 3000 rpm for 40 s. Finally, 8 nm of $MoO_3$ and 120 nm of Ag electrode were deposited by thermal evaporation through a shadow mask to form 0.075 $cm^2$ devices under a vacuum of $2 \times 10^{-6}$ mbar.

## Supporting Information

Supporting Information is available from the Wiley Online Library or from the author.

## Acknowledgements

This work was supported by the National Key Research Projects (Grant No. 2016YFA0202402), the National Natural Science Foundation of China (Grant Nos. 51761145013, 61911530158, 51803144, and 61674111), the Natural Science Foundation of Jiangsu Province of China (BK20170337), the China Postdoctoral Science Foundation (Grant No. 2019M651942), and "111" projects. The authors thank the Collaborative Innovation Center of Suzhou Nano Science and Technology, Soochow University, the Priority Academic Program Development of Jiangsu Higher Education Institutions (PAPD). This work was authored in part by the National Renewable Energy Laboratory, operated by Alliance for Sustainable Energy, LLC, for the U.S. Department of Energy (DOE) under Contract No. DE-AC36-08GO28308. The NREL authors acknowledge the Center for Hybrid Organic Inorganic Semiconductors for Energy (CHOISE), an Energy Frontier Research Center funded by the Office of Science, Office of Basic Energy Sciences within the U.S. Department of Energy. The views expressed in the article do not necessarily represent the views of the DOE or the U.S. Government.

## Conflict of Interest

The authors declare no conflict of interest.

## Keywords

$CsPbI_3$ quantum dots, di-*n*-propylamine, perovskite solar cells, surface ligand engineering

Received: January 19, 2020
Revised: May 26, 2020
Published online:

[1] J. Yuan, A. Hazarika, Q. Zhao, X. Ling, T. Moot, W. Ma, J. M. Luther, *Joule* **2020**, *4*, 1160.
[2] L. Protesescu, S. Yakunin, S. Kumar, J. Bär, F. Bertolotti, N. Masciocchi, A. Guagliardi, M. Grotevent, I. Shorubalko, M. I. Bodnarchuk, C.-J. Shih, M. V. Kovalenko, *ACS Nano* **2017**, *11*, 3119.
[3] T. Chiba, Y. Hayashi, H. Ebe, K. Hoshi, J. Sato, S. Sato, Y.-J. Pu, S. Ohisa, J. Kido, *Nat. Photonics* **2018**, *12*, 681.
[4] A. Hazarika, Q. Zhao, E. A. Gaulding, J. A. Christians, B. Dou, A. R. Marshall, T. Moot, J. J. Berry, J. C. Johnson, J. M. Luther, *ACS Nano* **2018**, *12*, 10327.
[5] L. Protesescu, S. Yakunin, M. I. Bodnarchuk, F. Krieg, R. Caputo, C. H. Hendon, R. X. Yang, A. Walsh, M. V. Kovalenko, *Nano Lett.* **2015**, *15*, 3692.
[6] Q. A. Akkerman, G. Rainò, M. V. Kovalenko, L. Manna, *Nat. Mater.* **2018**, *17*, 394.
[7] A. Swarnkar, A. R. Marshall, E. M. Sanehira, B. D. Chernomordik, D. T. Moore, J. A. Christians, T. Chakrabarti, J. M. Luther, *Science* **2016**, *354*, 92.
[8] M. Kulbak, S. Gupta, N. Kedem, L. Levine, T. Bendikov, G. Hodes, D. Cahen, *J. Phys. Chem. Lett.* **2016**, *7*, 167.
[9] P. Wang, X. Zhang, Y. Zhou, Q. Jiang, Q. Ye, Z. Chu, X. Li, X. Yang, Z. Yin, J. You, *Nat. Commun.* **2018**, *9*, 2225.
[10] J. Lin, M. Lai, L. Dou, C. S. Kley, H. Chen, F. Peng, J. Sun, D. Lu, S. A. Hawks, C. Xie, F. Cui, A. P. Alivisatos, D. T. Limmer, P. Yang, *Nat. Mater.* **2018**, *17*, 261.
[11] E. M. Sanehira, A. R. Marshall, J. A. Christians, S. P. Harvey, P. N. Ciesielski, L. M. Wheeler, P. Schulz, L. Y. Lin, M. C. Beard, J. M. Luther, *Sci. Adv.* **2017**, *3*, eaao4204.
[12] J. Yuan, X. Ling, D. Yang, F. Li, S. Zhou, J. Shi, Y. Qian, J. Hu, Y. Sun, Y. Yang, X. Gao, S. Duhm, Q. Zhang, W. Ma, *Joule* **2018**, *2*, 2450.
[13] X. Ling, S. Zhou, J. Yuan, J. Shi, Y. Qian, B. W. Larson, Q. Zhao, C. Qin, F. Li, G. Shi, C. Stewart, J. Hu, X. Zhang, J. M. Luther, S. Duhm, W. Ma, *Adv. Energy Mater.* **2019**, *9*, 1900721.

 © 2020 WILEY-VCH Verlag GmbH & Co. KGaA, Weinheim

[14] K. Ji, J. Yuan, F. Li, Y. Shi, X. Ling, X. Zhang, Y. Zhang, H. Lu, J. Yuan, W. Ma, *J. Mater. Chem. A* **2020**, *8*, 8104.
[15] M. Zhao, Y. Bai, S. Zeiske, L. Ren, J. Liu, Y. Yuan, N. Zarrabi, N. Chen, M. Ghasemi, P. Chen, M. Lyu, D. He, J.-H. Yun, Y. Du, Y. Wang, S. Ding, A. Armin, P. Meredith, G. Liu, H.-M. Cheng, L. Wang, *Nat. Energy* **2020**, *5*, 79.
[16] J. Yuan, Y. Zhang, L. Zhou, G. Zhang, H.-L. Yip, T.–K. Lau, X. Lu, C. Zhu, H. Peng, P. A. Johnson, M. Leclerc, Y. Cao, J. Ulanski, Y. Li, Y. Zou, *Joule* **2019**, *3*, 1140.
[17] M. Kim, G.-H. Kim, T. K. Lee, I. W. Choi, H. W. Choi, Y. Jo, Y. J. Yoon, J. W. Kim, J. Lee, D. Huh, H, Lee , S. K. Kwak, J. Y. Kim, D. S. Kim, *Joule* **2019**, *3*, 2179.
[18] F. Li, S. Zhou, J. Yuan, C. Qin, Y. Yang, J. Shi, X. Ling, Y. Li, W. M, *ACS Energy Lett.* **2019**, *4*, 2571.
[19] E. A. Gaulding, J. Hao, H. S. Kang, E. M. Miller, S. N. Habisreutinger, Q. Zhao, A. Hazarika, P. C. Sercel, J. M. Luther, J. L. Blackburn, *Adv. Mater.* **2019**, *31*, 1902250.
[20] L. M. Wheeler, E. M. Sanehira, A. R. Marshall, P. Schulz, M. Suri, N. C. Anderson, J. A. Christians, D. Nordlund, D. Sokaras, T. Kroll, S. P. Harvey, J. J. Berry, L. Y. Lin, J. M. Luther, *J. Am. Chem. Soc.* **2018**, *140*, 10504.
[21] M. Liu, O. Voznyy, R. Sabatini, F. P. García de Arquer, R. Munir, A. H. Balawi, X. Lan, F. Fan, G. Walters, A. R. Kirmani, S. Hoogland, F. Laquai, A. Amassian, E. H. Sargent, *Nat. Mater.* **2017**, *16*, 258.
[22] J. Xu, O. Voznyy, M. Liu, A. R. Kirmani, G. Walters, R. Munir, M. Abdelsamie, A. H. Proppe, A. Sarkar, F. P. García de Arquer, *Nat. Nanotechnol.* **2018**, *13*, 456.
[23] M. Liu, Y. Chen, C.-S. Tan, R. Q. Bermudez, A. H. Proppe, R. Munir, H. Tan, O. Voznyy, B. Scheffel, G. Walters, A. P. T. Kam, B. Sun, M.-J. Choi, S. Hoogland, A. Amassian, S. O. Kelley, F. P. García de Arquer, E. H. Sargent, *Nature* **2019**, *570*, 96.
[24] N. C. Anderson, M. P. Hendricks, J. J. Choi, J. S. Owen, *J. Am. Chem. Soc.* **2013**, *135*, 18536.
[25] J. E. Tackett, *Appl. Spectrosc.* **1989**, *43*, 483.
[26] D. M. Kroupa, M. Voros, N. P. Brawand, B. W. McNichols, E. M. Miller, J. Gu, A. J. Nozik, A. Sellinger, G. Galli, M. C. Beard, *Nat. Commun.* **2017**, *8*, 15257.
[27] Z. Zhu, Y. Bai, X. Liu, C.-C. Chueh, S. Yang, A. K.-Y. Jen, *Adv. Mater.* **2016**, *28*, 6478.
[28] C. Li, S. Tscheuschner, F. Paulus, P. E. Hopkinson, J. Kießling, A. Köhler, Y. Vaynzof, S. Huettner, *Adv. Mater.* **2016**, *28*, 2446.
[29] J. Shi, J. Dong, S. Lv, Y. Xu, L. Zhu, J. Xiao, X. Xu, H. Wu, D. Li, Y. Luo, Q. Meng, *Appl. Phys. Lett.* **2014**, *104*, 063901.
[30] S. M. Sze, K. K. Ng, *Physics of Semiconductor Devices*, 3rd ed., Wiley, New York **2006**.
[31] J. Tian, Q. Xue, X. Tang, Y. Chen, N. Li, Z. Hu, T. Shi, X. Wang, F. Huang, C. J. Brabec, H. L. Yip, Y. Cao, *Adv. Mater.* **2019**, *31*, 1901152.
[32] A. J. Ferguson, N. Kopidakis, S. E. Shaheen, G. Rumbles, *J. Phys. Chem. C* **2011**, *115*, 23134.
[33] L. E. Garner, A. Bera, B. W. Larson, D. P. Ostrowski, A. J. Pal, W. A. Braunecker, *ACS Energy Lett.* **2017**, *2*, 1556.
[34] Y. Xu, J. Yuan, S. liang, J.-D. Chen, Y. Xia, B. W. Larson, Y. Wang, G. M. Su, Y. Zhang, C. Cui, M. Wang, H. Zhao, W. Ma, *ACS Energy Lett.* **2019**, *4*, 2277.
[35] J. Rivnay, S. C. Mannsfeld, C. E. Miller, A. Salleo, M. F. Toney, *Chem. Rev.* **2012**, *112*, 5488.
[36] F. Li, J. Yuan, X. Ling, Y. Zhang, Y. Yang, S. H. Cheung, C. H. Y. Ho, X. Gao, W. Ma, *Adv. Funct. Mater.* **2018**, *28*, 1706377.
[37] J. D. Roo, M. Ibáñez, P. Geiregat, G. Nedelcu, W. Walravens, J. Maeos, J. C. Martins, I. V. Driessche, M. V. Kovalenko, Z. Hens, *ACS Nano* **2016**, *10*, 2071.
[38] G. Almeida, I. Infante, L. Manna, *Science* **2019**, *364*, 833.
[39] D. Bai, J. Zhang, Z. Jin, H. Bian, K. Wang, H. Wang, L. Liang, Q. Wang, S. F. Liu, *ACS Energy Lett.* **2018**, *3*, 970.
[40] F. Liu, Y. Zhang, C. Ding, S. Kobayashi, T. Izuishi, N. Nakazawa, T. Toyoda, T. Ohta, S. Hayase, T. Minemoto, K. Yoshino, S. Dai, Q. Shen, *ACS Nano* **2017**, *11*, 10373.
[41] A. Yella, L. P. Heiniger, P. Gao, M. K. Nazeeruddin, M. Gratzel, *Nano Lett.* **2014**, *14*, 2591.


© 2020 WILEY-VCH Verlag GmbH & Co. KGaA, Weinheim